

One-step rapid fabrication of paper-based microfluidic devices using fluorocarbon plasma polymerization

Peng-Kai Kao · Cheng-Che Hsu

Received: 31 August 2013 / Accepted: 18 January 2014 / Published online: 28 January 2014
© Springer-Verlag Berlin Heidelberg 2014

Abstract In this work, we demonstrated an all-dry, top-down, and one-step rapid process to fabricate paper-based microfluidic devices using fluorocarbon plasma polymerization. This process is able to create fluorocarbon-coated hydrophobic patterns on filter paper substrates while maintaining the trench and detection regions intact and free of contamination after the fabrication process, as confirmed by attenuated total reflectance–Fourier transform infrared spectroscopy and X-ray photoelectron spectroscopy. We have shown that the processing time is one critical factor that influences the device performance. For the device fabricated with a sufficiently long processing time (180 s), the sample fluid flow can be well confined in the patterned trenches. By testing the device with an 800 μm channel width, a sample solution amount as small as 4.5 μL is sufficient to perform the test. NO_2^- assay is also performed and shows that such a device is capable for biochemical analysis.

1 Introduction

Over the past few years, there has been an upsurge of interest in the development of paper-based microfluidic devices used for biochemical, environmental, and general health applications (Ballerini et al. 2012; Choi et al. 2011; Cheng et al. 2010). Paper-based microfluidic devices can be built by demarcating hydrophilic paper by hydrophobic barriers. Compared with conventional microfluidic devices, paper-based microfluidic devices are great candidate in

point-of-care device in developing countries because they are low cost, easy to process, available in abundance, disposable, and no pumps are required to transport fluids on a porous paper substrate due to capillary action (Martinez 2011). A promising paper-based microfluidic device was introduced by Whitesides group at Harvard University using the photolithographic process (Martinez et al. 2007). Since then, there has been a great number of literatures reporting fabrication of paper-based microfluidic devices using different techniques, such as ink-jet printing (Abe et al. 2008), plasma-assisted fabrication (Li et al. 2008, 2010), wax printing (Carrilho et al. 2009), plotting (Bruzewicz et al. 2008), flexographic printing (Olkkonen et al. 2010), and cutting (Cassano and Fan 2013; Fu et al. 2011). Significant progress has been made and a top-down, all-dry, and one-step rapid fabrication process with good pattern transfer fidelity is highly desired. Such a process is efficient and cost effective. Particularly, an all-dry process allows for the fluidic channel and the detection region remaining intact and free of potential contamination by wet chemicals during the fabrication steps. Among various types of fabrication processes, whether or not the chemical composition of the detection region (and/or the fluid channel) on the paper substrate remains unchanged after the fabrication process is still unexplored.

In this work, we report an all-dry and rapid one-step process to fabricate paper-based microfluidic devices using fluorocarbon plasma polymerization. By using octafluorocyclobutane ($\text{c-C}_4\text{F}_8$) as the precursor, paper-based microfluidic devices, i.e., filter paper substrates with fluorocarbon-containing-polymer-coated area as hydrophobic boundaries, can be fabricated. We utilize Fourier transform infrared spectroscopy (FTIR) and X-ray photoelectron spectroscopy (XPS) to examine the chemical composition of coated and uncoated areas on the paper

P.-K. Kao · C.-C. Hsu (✉)
Department of Chemical Engineering,
National Taiwan University, Taipei, Taiwan
e-mail: chsu@ntu.edu.tw

substrate. The effect of the deposition time on the device performance is studied. Finally, NO_2^- assay is performed to test the fabricated paper-based device.

2 Experimental section

2.1 Materials

In this work, NO_2^- assay was utilized for quantitative analyses. The NO_2^- stock solution was prepared by dissolving sodium nitrite (99 %, Sigma-Aldrich) in deionized water. The NO_2^- indicator contains 10 mmol/L *N*-(1-naphthyl) ethylenediamine (98 %, Sigma-Aldrich), 50 mmol/L sulfanilamide (99 %, Sigma-Aldrich), and 330 mmol/L citric acid (99.5 %, Sigma-Aldrich) (Blicharz et al. 2008). The dye solution used for fluid transportation observation was prepared by dissolving Orange II (Acros) in deionized water. All chemicals are used as received without further purification.

Whatman filter paper (No. 2) was used as the paper substrate. The filter paper was sandwiched between two metal masks and subsequently exposed to the plasma to deposit fluorocarbon films in a plasma reactor. Metal masks were made by mechanically cutting of stainless steel sheets 2 mm in thickness. The dimensions of the stainless steel mask are as follow: channel width 1 mm and channel length 7.5 mm with detection region 3 mm \times 3 mm. The two masks are aligned manually. The paper substrate is tightly sandwiched between the two masks to minimize the space between the metal mask and the paper. A thick mask (2 mm) has been used to ensure a close contact between the mask and the paper substrate in the patterned region, which is critical for good pattern transfer fidelity. The mask on the top of the filter paper was a positive mask, while the one beneath the paper was a negative mask as shown in Fig. 1a. The positive (top) mask serves as the mask to define the channel and detection areas and to ensure trench and detecting area remaining intact during the process. The negative (bottom) mask allows for the deposition of hydrophobic fluorocarbon films on the bottom of the channel and detection areas. Such a two-side deposition allows for a better confinement of the analyte within the trench and detection areas, which gives higher pattern transfer fidelity. This also ensures that the channel is well confined by hydrophobic boundaries, as shown in Fig. 1b. The cross-section view of the treated paper trench area shown here also indicates that the trench region is confined at the upper surface of the substrate. It also shows that the vertical penetration depth of the deposition species is approximately 120 μm . We note that the penetration depth is a strong function of the processing time and plasma conditions, and this depth is obtained using the present operating condition.

2.2 Plasma polymerization process

The plasma system used was a parallel-plate capacitively coupled discharge sustained by a 13.56 MHz power source (CAESAR 136) with an L-type matching network. The electrode diameters of the two parallel plates are 15 cm, and the gap between the top and bottom electrodes is 6 cm. The bottom electrode is the powered electrode, while the top electrode is grounding. After placing a sample on the powered electrode, the reactor was evacuated to base pressure (<0.1 mTorr). The deposition gas mixture consisted of a precursor gas (*c*- C_4F_8 flowing at 1 sccm) and an inert gas (argon flowing at 50 sccm). The process pressure is 130 mTorr, and the RF power applied to the powered electrode is 15–50 W. A schematic illustration of this one-step paper-based microfluidic device fabrication method is shown in Fig. 1b.

2.3 Chemical characterization of the coated films

FTIR analysis was performed with an IR spectrometer (Perkin Elmer spectrum 100) equipped with a liquid-nitrogen-cooled mercury-cadmium-telluride detector in the attenuated total reflectance (ATR) mode. XPS (Thermo Scientific, Theta Probe) analysis was performed using a monochromated Al $K\alpha$ x-ray source.

2.4 Data processing

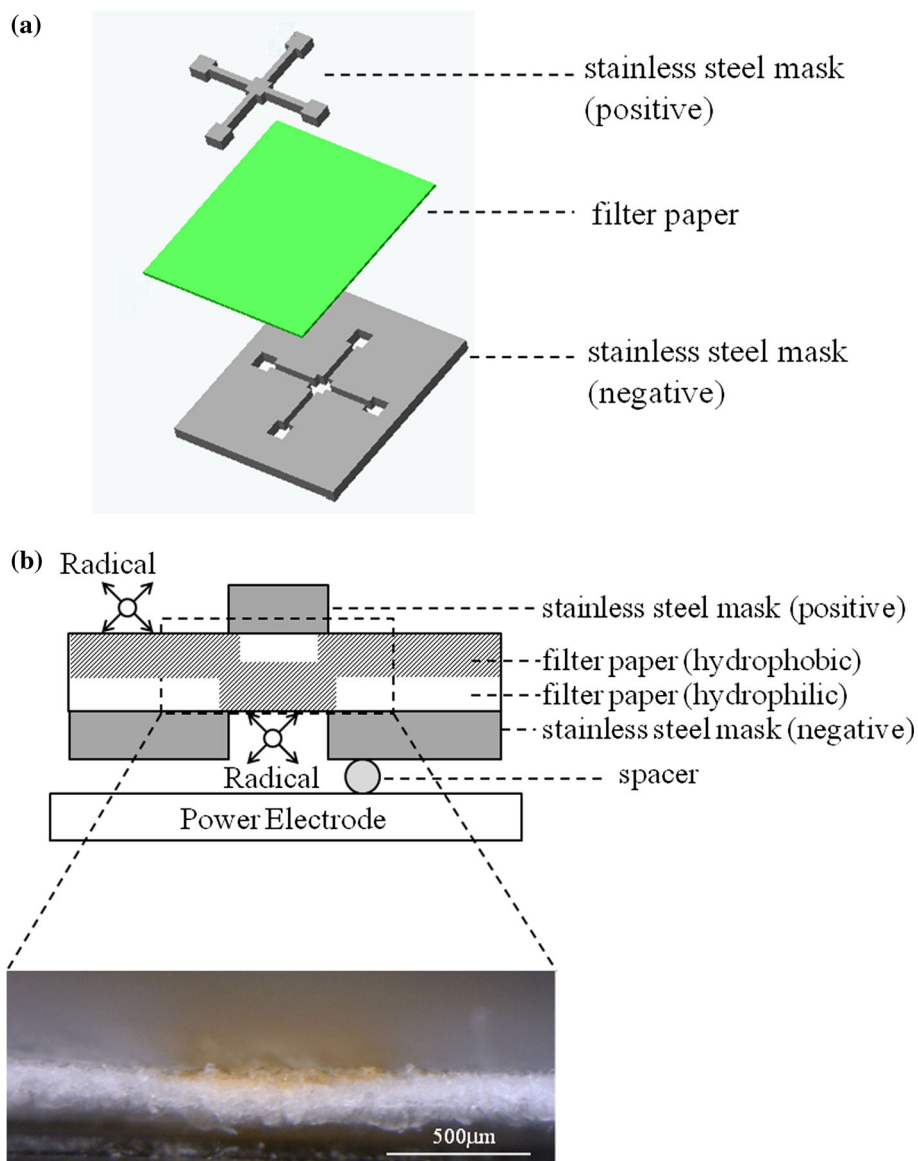
To quantify the color response of the NO_2^- assay, we perform a color scan of the device using a commercially available scanner (HP, Deskjet F4280 Printer) after the analyte is applied to the test device for 5 min. The scanned image was then deconvoluted using the color image obtained from the detection region into red (R), green (G), and blue (B) components. Two processing schemes using this RGB components are tested to quantify the color image. The first scheme (scheme I) is summarizing the normalized RGB components, as an indicator of the “brightness” of this image. The scheme weights RGB components equally and is somewhat different from the gray scale, which weights RGB components differently. The second scheme (scheme II) is to take the ratio of $R/(R+G+B)$ as the quantification, since the colorimetric output produced from the NO_2^- assay is a red-violet azo compound (Blicharz et al. 2008).

3 Results and discussion

3.1 One-step paper patterning by plasma polymerization

Figure 2 shows the visual appearance of a set of the microfluidic pattern on a paper substrate after 10 μL of

Fig. 1 Schematic of the fabrication process of the paper-based microfluidic devices using fluorocarbon plasma polymerization: **a** the geometric design of the stainless steel masks and **b** the cross-sectional illustration of the plasma polymerization process and the photo image of the cross-section of the treated paper trench area. *Notes* (i) the schematic is not drawn in scale, (ii) in this photo image, dye solution is applied to the trench area to visualize the hydrophilic and hydrophobic areas



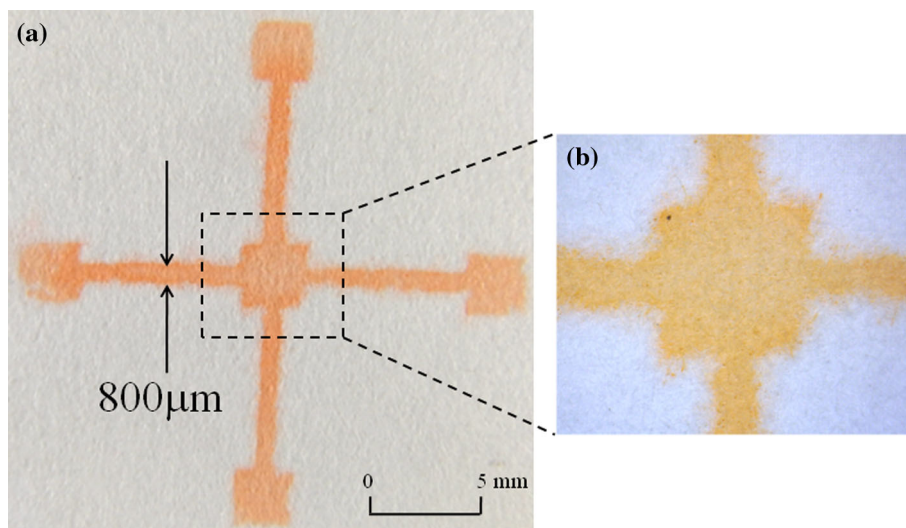
Orange II dye solution is absorbed. This microfluidic pattern was fabricated with 150 s of deposition time with the RF power of 15 W. Ten microliters of the dye solution is applied into the central square of the patterned paper. It is shown that after absorbing 10 µL of the solution by the capillary force, the dye solution is nearly fully confined in the microfluidic channel with very little leak outside of the channel. The flow of the dye solution shows that the fluid transports in all four directions but with slight variation in the transportation speeds. With a stainless steel mask 1 mm in width in the trench area, 800 µm-wide trenches can be obtained. Such a slightly smaller patterned trench width compared with the mask is a result of the lateral diffusion of the deposition species such as CF₂. We note that a smaller trench width can be obtained using a mask with a thinner trench width. Given

the lateral and vertical diffusion of the deposition species, the smallest trench width can be fabricated using this process is 300–500 µm. Based on the comparison made by Martinez et al. (2009), such a resolution and feature transfer fidelity is inferior to photolithographic processes, but is comparable or superior to several other processes such as wax printing, plotting, inkjet etching, plasma etching, and cutting.

3.2 Chemical analysis of the patterned paper

To perform chemical analysis of the patterned paper, ATR-FTIR and XPS are utilized. ATR-FTIR is able to analyze the property of the paper substrate at the top surface hundreds of nm to a few µm deep. XPS analysis is aimed for the compositional analysis at the very surface, few nm

Fig. 2 Pattern of the device fabricated by fluorocarbon plasma polymerization under the following condition: $c\text{-C}_4\text{F}_8$ (1 sccm)/Ar(50 sccm), RF power 15 W, and 150 s processing time **a** the front side of the device with 800 μm microfluidic channel wetted by dye solution and **b** the magnification of the image in **(a)**



deep, of the paper surface. Comparing with XPS, ATR–FTIR analysis reveals the compositional information more toward the “bulk” of the paper substrate.

We first use ATR–FTIR to identify the carbon- and fluorine-containing bonding of the paper substrate. The untreated filter paper, the detection region (covered by the mask), and the hydrophobic area (coated region) are examined. The ATR–FTIR spectra shown in Fig. 3a indicate typical IR spectra of the filter paper: O–H stretching vibration region from 3,200 to 3,500 cm^{-1} , C–O–C asymmetric vibration in cellulose at 1,162–1,125 cm^{-1} , and C–O stretch in cellulose at 1,030–1,060 cm^{-1} (Schwanninger et al. 2004). It is worthy to note that all the spectra shown here are nearly identical, and no CF-related signal is observed in the detection region, which suggests that the deposited layer thickness is few hundreds of nm or thinner. The variation among these three spectra is within 5 %. This observation shows two important features of this proposed process: (i) the major chemical composition of the filter paper remains intact, even with plasma treatment; (ii) it only requires a thin fluorocarbon layer for the device to work, guaranteeing the efficiency of the process.

In order to exam the chemical composition of the deposited films, and to further confirm that the detection area remains intact after the deposition process, we used a condition ($c\text{-C}_4\text{F}_8/\text{Ar} = 30/50$ sccm and RF power 30 W) that is $c\text{-C}_4\text{F}_8$ richer with elongated treatment time (30 min) to perform the paper substrate treatment using the same set of masks. This condition allows for the plasma polymerization occurring at a higher deposition rate and forming a much thicker deposited layer, which is detectable by ATR–FTIR. Figure 3b shows the ATR–FTIR spectra of the detection and the hydrophobic regions. We first note that even under this selected condition with an elongated processing time, the spectrum of the detection

region remains nearly identical with the untreated filter paper. In the spectrum of the hydrophobic region, a strong CF_x ($x = 1, 2, \text{ and } 3$) stretching modes between 1,100 and 1,400 cm^{-1} appears. This band mostly appears in an amorphous cross-linked fluorocarbon film (Favia et al. 2003). In addition, the characteristic signals of O–H band and C–O stretch in cellulose (paper substrate) are still seen, but with lower intensities.

To further analyze the surface composition of the paper substrate, XPS spectra are examined. C(1s) and F(1s) spectra of untreated filter paper, the detection region, and the hydrophobic area are examined, and Fig. 4 shows the results. The C(1s) spectrum of the untreated filter paper can be deconvoluted into C–C/C–H (binding energy (B.E.) ~ 285.0 eV) and C–O (B.E. ~ 286.6 eV). The most noticeable peak, C–O, is most likely related to the C–O bond of cellulose or the paper sizing agents remained in the matrix surrounding between microfibrils. For the detection region, a nearly identical C(1s) spectrum comparing with the untreated filter paper is observed. This shows that the chemical composition of the detection region remains the same as the untreated filter paper. The C(1s) spectrum of the hydrophobic region clearly shows CF (B.E. ~ 289.0 eV), CF_2 (B.E. ~ 292.0 eV), and CF_3 (B.E. ~ 294.0 eV) bindings, which clearly demonstrates the occurrence of fluorocarbon plasma polymerization (Martin et al. 2004) at the paper surface. The F(1s) spectra show that both the filter paper and the detection region are free of fluorine, while the fluorine exists in the hydrophobic area. Based on XPS and FTIR analysis, we believe that this process allows for fabrication of paper-based microfluidics devices with fluorocarbon-based hydrophobic barriers while keeping chemical composition of the trench and detection area nearly identical as the untreated filter paper. Such a process feature makes it unique comparing with processes that the whole

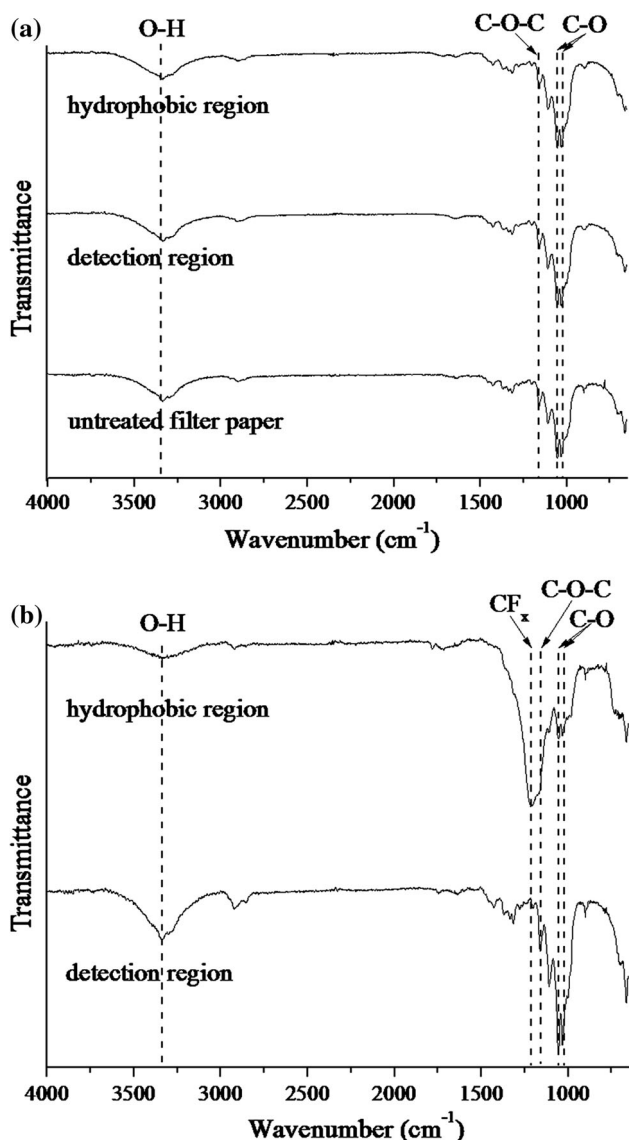


Fig. 3 The FTIR spectra of different regions of treated and untreated paper under different processing condition: **a** $c\text{-C}_4\text{F}_8$ (1 sccm)/Ar (50 sccm), 15 W RF power for 30 s, and **b** $c\text{-C}_4\text{F}_8$ (30 sccm)/Ar(50 sccm), 30 W RF power for 30 min plasma polymerization

paper is coated with hydrophobic agent, and selected area is treated and becomes hydrophilic (Abe et al. 2008; Li et al. 2008). The left of agent residue on the paper substrate after the treatment potentially interferes in the following analysis step, especially when the agent residue is not inert.

3.3 Parametric study: effect of processing time on fluid transportation behavior

The requirement of the sample solution amount and the confinement of the test solution in the channel during transportation are two critical elements for paper-based microfluidics. It is found that the plasma processing time is

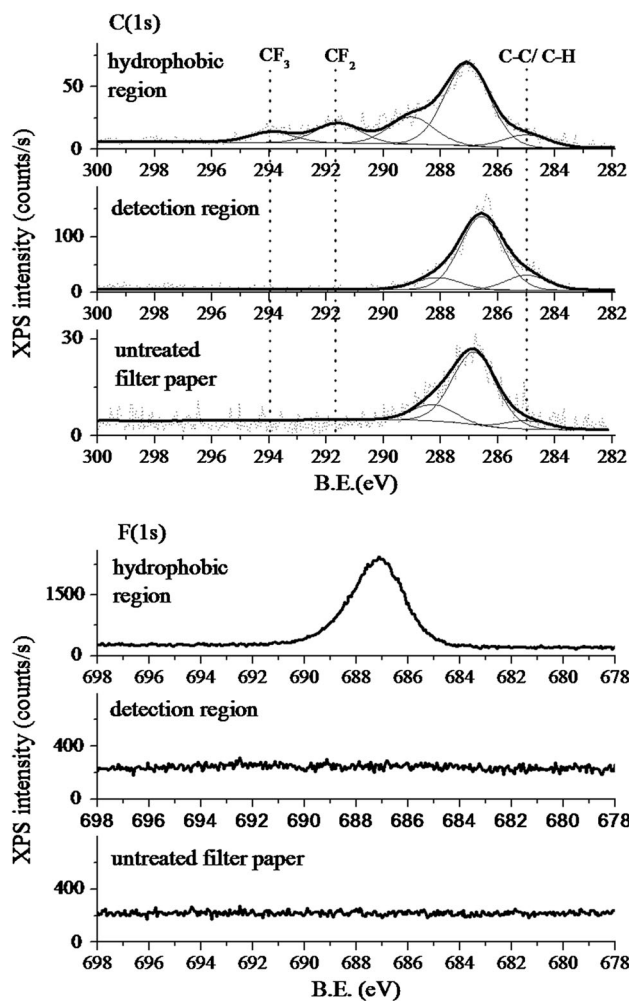


Fig. 4 XPS C(1s) and F(1s) spectra of fluorocarbon deposited hydrophobic region and detection region on a paper substrate using $c\text{-C}_4\text{F}_8$ (1 sccm)/Ar(50 sccm), 30 s, and power input 15 W. The spectra of untreated filter paper are also shown

one of the key parameters that influence the device performance. To test how the processing time for plasma polymerization influences the fluid transportation behavior, devices fabricated with different processing time are examined. Dye solution (Orange II dissolved in deionized water) is initially applied into the central area drop by drop, allowed for the solution flowing through the channels, and reaching the detection regions. The amount of sample solution required is defined by the minimal solution volume applied to completely wet one channel and reach the detection region. As shown in Fig. 5a, the volume of sample solution used decreases significantly from 25 to 4.5 μL as the processing time increases from 15 to 180 s. The patterned trench width decreases slightly with the increase in the process time due to the lateral diffusion of fluorocarbon-containing species during the process, as noted earlier. This observation shows that the lateral diffusion does not significantly deteriorate the pattern transfer

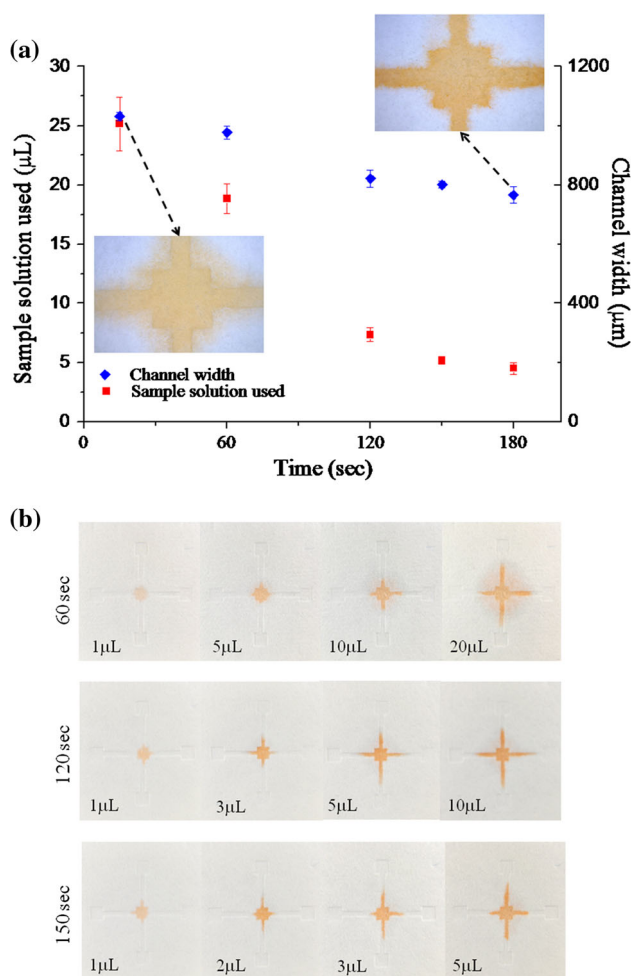


Fig. 5 **a** Effect of plasma processing time on sample solution required and patterned channel width under the plasma condition of $c\text{-C}_4\text{F}_8$ (1 sccm)/Ar(50 sccm) with RF power input of 15 W. **b** Series of photographs taken for visualizing sample solution transported in patterned paper made with different plasma processing time: 60, 120, and 150 s

fidelity. This is superior to processes that require the spreading of liquid phase agent into paper substrate to define the microfluidic channels, such as wax printing. Due to the anisotropic nature of paper substrate, lateral spreading of liquid agent in the paper substrate is usually more rapid than vertical spreading, as stated by Carrilho et al. Such a lateral spreading results in inferior pattern transfer fidelity as opposed to the plasma polymerization process proposed in this work. We also observe that for the device fabricated with insufficiently long plasma processing time, the sample solution is not well confined in the channel and “leaks” out to the hydrophobic region. In order for the solution to fully wet the channel and to reach the detection area, it needs a larger amount of sample solution. Under such a situation, it is not only wasting the sample solution, but also not suitable for practical applications. When the processing time is sufficiently long, i.e.,

180 s, the fluid is well confined in the channel and it only requires a minimal amount, 4.5 μL, of sample solution to wet the channel and to reach the detection area. Figure 5b shows series of photographs taken to visualize the transportation of sample solution in the patterned filter paper fabricated under different processing time. It is clearly shown that it only requires a single step and 180 s of processing time to fabricate a paper-based microfluidics device with desired hydrophobic patterns. It also shows that such a device demonstrates good pattern transfer fidelity, which is a key feature of plasma-based processes.

3.4 Quantitative analysis

In order to test the paper-based microfluidic devices for quantitative biochemical analyses, we perform NO_2^- assay using devices fabricated by plasma polymerization. NO_2^- was chosen as the analyte since it is a reliable biological marker for many human health conditions (Nagler 2008). We first applied 7 μL of NaNO_2 solution with concentrations of 10, 5, 1.5, 0.25 mM to the central area of four devices. The color images of these tested devices are shown in Fig. 6. The different color responses of the analytes with different concentration are clearly observed. The color responses in the four detection areas are reasonably uniform, proving the performance in test solution transportation on this device. The color response is then

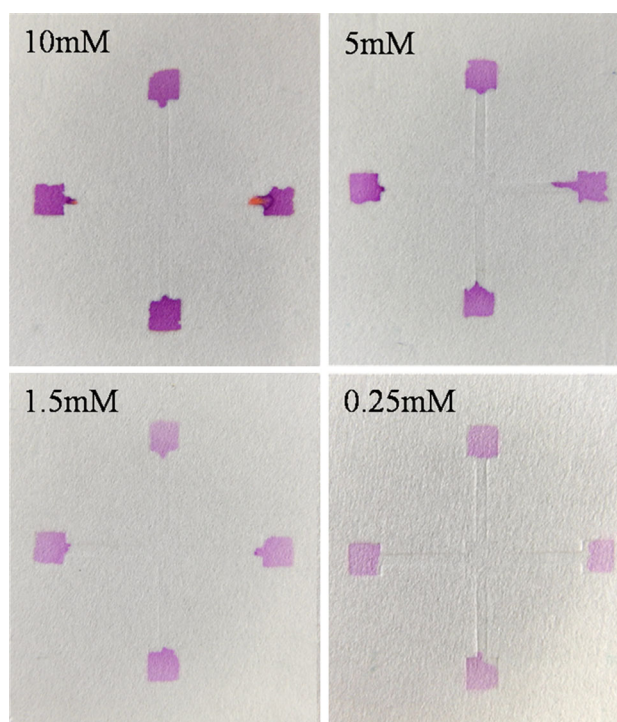


Fig. 6 Color response of NO_2^- assay on the patterned paper for NaNO_2 concentration of 10, 5, 1.5, and 0.25 mM

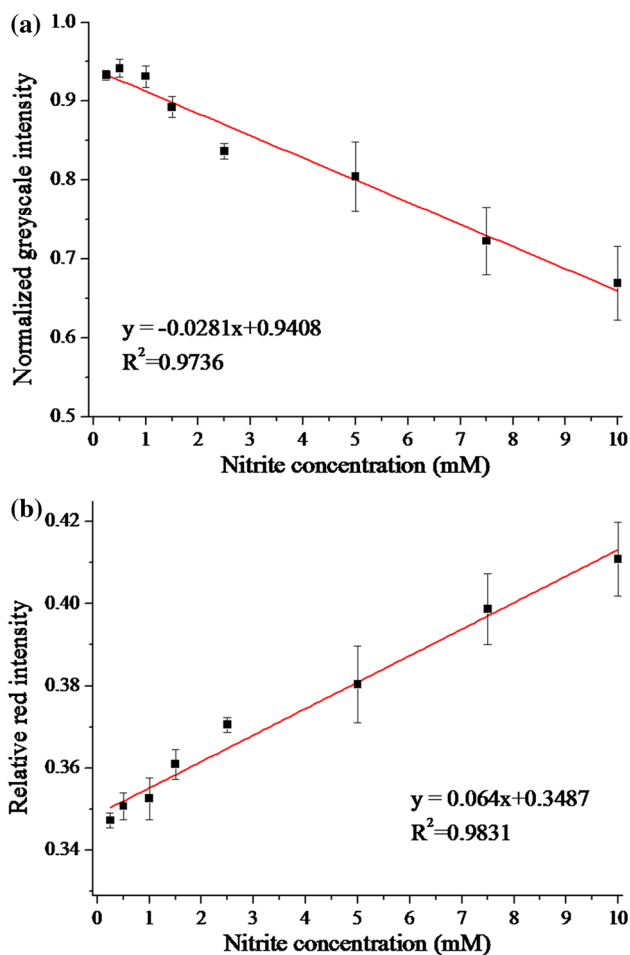


Fig. 7 Calibration curve for nitrite solution with **a** scheme I and **b** scheme II for color quantification

analyzed by the two schemes described in the experimental section. The calibration curves obtained by using two color analysis schemes are shown in Fig. 7. Fitting using linear regression analysis is also performed. The R^2 values for scheme I and II are 0.97 and 0.98, respectively. In this calibration curve, we intentionally test a range of NO_2^- concentration up to 10 mM, which is a wider range comparing with those reported in the literature [e.g., up to 1.3 mM in the work reported by Klasner et al. (2010) and Li et al. (2010)]. The purpose for the test over a wider range is to further understand our device behavior, rather than comparing the device performance with those reported in the literature. For this set of test, we choose identical analyte and indicator concentrations as those reported by Klasner et al. (2010), with an analyte to indicator volume ratio of 3.5. This ratio is smaller than that used in Klasner's work, which has an analyte to indicator volume ratio of 10. Such a relatively smaller amount of analyte usage is relevant to the geometric design of the microfluidic pattern. It prevents the complete consumption of the indicator,

leading to a linear response over a wide range up to 10 mM. This demonstrates that the process proposed in this work is capable of fabricate paper-based microfluidics devices with reasonable performance.

4 Conclusions

In this work, we demonstrated a process to fabricate paper-based microfluidics devices using plasma processing. This process uses a physical mask to perform plasma polymerization by forming hydrophobic fluorocarbon-based regions on paper substrates. This is a top-down, all-dry, and rapid process to fabricate paper-based microfluidic devices in one step. While this process is able to create fluorocarbon-coated patterns on paper substrates, the trench and detection regions remain intact and free of contamination after the fabrication process, as confirmed by ATR-FTIR and XPS. As shown above, this process demonstrates good pattern transfer fidelity, which is a key feature of plasma processes. Given the above-mentioned process advantages, the disadvantages of this process are the requirement of different masks for different channel design as well as the high cost of the plasma system. We note that in spite of the high plasma equipment cost, one key feature of dry processes is the smaller amount of chemical usage as opposed to wet processes. We have assessed the effect of the processing time on the device performance and found that it is a very critical factor. With sufficiently long processing time (180 s), the patterned trenches are able to strictly confine the transport of the sample solution. By testing devices with 800 μm channel width, a sample amount as small as 5 μL is sufficient to fully wet the trench and to reach the detection region. NO_2^- assay is also performed and shows a reasonable performance. It is demonstrated that such a device is capable for biochemical analysis.

Acknowledgments This work is supported by National Science Council, Taiwan (101-2221-E-002-163-MY2 and 102-3113-P-002-043).

References

- Abe K, Suzuki K, Citterio D (2008) Inkjet-printed microfluidic multianalyte chemical sensing paper. *Anal Chem* 80(18): 6928–6934. doi:10.1021/AC800604v
- Ballerini DR, Li X, Shen W (2012) Patterned paper and alternative materials as substrates for low-cost microfluidic diagnostics. *Microfluid Nanofluid* 13(5):769–787. doi:10.1007/s10404-012-0999-2
- Blicharz TM, Rissin DM, Bowden M, Hayman RB, DiCesare C, Bhatia JS, Grand-Pierre N, Siqueira WL, Helmerhorst EJ, Loscalzo J, Oppenheim FG, Walt DR (2008) Use of colorimetric test strips for monitoring the effect of hemodialysis on salivary nitrite and uric acid in patients with end-stage renal disease: a

- proof of principle. *Clin Chem* 54(9):1473–1480. doi:[10.1373/clinchem.2008.105320](https://doi.org/10.1373/clinchem.2008.105320)
- Bruzewicz DA, Reches M, Whitesides GM (2008) Low-cost printing of poly(dimethylsiloxane) barriers to define microchannels in paper. *Anal Chem* 80(9):3387–3392. doi:[10.1021/Ac702605a](https://doi.org/10.1021/Ac702605a)
- Carrilho E, Martinez AW, Whitesides GM (2009) Understanding wax printing: a simple micropatterning process for paper-based microfluidics. *Anal Chem* 81(16):7091–7095. doi:[10.1021/Ac901071p](https://doi.org/10.1021/Ac901071p)
- Cassano CL, Fan ZH (2013) Laminated paper-based analytical devices (LPAD): fabrication, characterization, and assays. *Microfluid Nanofluid* 15(2):173–181. doi:[10.1007/s10404-013-1140-x](https://doi.org/10.1007/s10404-013-1140-x)
- Cheng CM, Martinez AW, Gong JL, Mace CR, Phillips ST, Carrilho E, Mirica KA, Whitesides GM (2010) Paper-based ELISA. *Angew Chem Int Ed* 49(28):4771–4774. doi:[10.1002/anie.201001005](https://doi.org/10.1002/anie.201001005)
- Choi S, Goryll M, Sin LYM, Wong PK, Chae J (2011) Microfluidic-based biosensors toward point-of-care detection of nucleic acids and proteins. *Microfluid Nanofluid* 10(2):231–247. doi:[10.1007/s10404-010-0638-8](https://doi.org/10.1007/s10404-010-0638-8)
- Favia P, Cicala G, Milella A, Palumbo F, Rossini R, d'Agostino R (2003) Deposition of super-hydrophobic fluorocarbon coatings in modulated RF glow discharges. *Surf Coat Tech* 169:609–612. doi:[10.1016/S0257-8972\(03\)00123-3](https://doi.org/10.1016/S0257-8972(03)00123-3)
- Fu EL, Ramsey S, Kauffman P, Lutz B, Yager P (2011) Transport in two-dimensional paper networks. *Microfluid Nanofluid* 10(1):29–35. doi:[10.1007/s10404-010-0643-y](https://doi.org/10.1007/s10404-010-0643-y)
- Klasner SA, Price AK, Hoeman KW, Wilson RS, Bell KJ, Culbertson CT (2010) Paper-based microfluidic devices for analysis of clinically relevant analytes present in urine and saliva. *Anal Bioanal Chem* 397(5):1821–1829. doi:[10.1007/s00216-010-3718-4](https://doi.org/10.1007/s00216-010-3718-4)
- Li X, Tian J, Nguyen T, Shen W (2008) Paper-based microfluidic devices by plasma treatment. *Anal Chem* 80(23):9131–9134. doi:[10.1021/ac801729t](https://doi.org/10.1021/ac801729t)
- Li X, Tian J, Shen W (2010) Progress in patterned paper sizing for fabrication of paper-based microfluidic sensors. *Cellulose* 17(3):649–659. doi:[10.1007/s10570-010-9401-2](https://doi.org/10.1007/s10570-010-9401-2)
- Martin IT, Malkov GS, Butoi CI, Fisher ER (2004) Comparison of pulsed and downstream deposition of fluorocarbon materials from C3F8 and c-C4F8 plasmas. *J Vac Sci Technol A* 22(2):227–235. doi:[10.1116/1.1638779](https://doi.org/10.1116/1.1638779)
- Martinez AW (2011) Microfluidic paper-based analytical devices: from POKET to paper-based ELISA. *Bioanalysis* 3(23):2589–2592. doi:[10.4155/Bio.11.258](https://doi.org/10.4155/Bio.11.258)
- Martinez AW, Phillips ST, Butte MJ, Whitesides GM (2007) Patterned paper as a platform for inexpensive, low-volume, portable bioassays. *Angew Chem Int Ed* 46(8):1318–1320. doi:[10.1002/anie.200603817](https://doi.org/10.1002/anie.200603817)
- Martinez AW, Phillips ST, Whitesides GM, Carrilho E (2009) Diagnostics for the developing world: microfluidic paper-based analytical devices. *Anal Chem* 82(1):3–10. doi:[10.1021/ac9013989](https://doi.org/10.1021/ac9013989)
- Nagler RM (2008) Saliva analysis for monitoring dialysis and renal function. *Clin Chem* 54(9):1415–1417. doi:[10.1373/clinchem.2008.112136](https://doi.org/10.1373/clinchem.2008.112136)
- Olkkonen J, Lehtinen K, Erho T (2010) Flexographically printed fluidic structures in paper. *Anal Chem* 82(24):10246–10250. doi:[10.1021/Ac1027066](https://doi.org/10.1021/Ac1027066)
- Schwanninger M, Rodrigues JC, Pereira H, Hinterstoisser B (2004) Effects of short-time vibratory ball milling on the shape of FT-IR spectra of wood and cellulose. *Vib Spectrosc* 36(1):23–40. doi:[10.1016/j.vibspec.2004.02.003](https://doi.org/10.1016/j.vibspec.2004.02.003)